





Article

Image-Enhanced Pseudo-Thermal Ghost Imaging with Hybrid Speckle Pattern

Tong Tian ^{1,2,†} , Zhe Sun ^{1,2,*,†} , Sukyoon Oh ^{1,2}  and Christian Spielmann ^{1,2,*} 

¹ Institute of Optics and Quantum Electronics, Abbe Center of Photonics, Friedrich Schiller University, Max Wien Platz 1, 07743 Jena, Germany; tong.tian@uni-jena.de (T.T.)

² Helmholtz Institute Jena, Fröbelstieg 3, 07743 Jena, Germany

* Correspondence: sunzhe@nwpu.edu.cn (Z.S.); christian.spielmann@uni-jena.de (C.S.)

† These authors contributed equally to this work.

Abstract: In this study, the influence of hybrid speckle patterns on the contrast-to-noise ratio (CNR) and resolution in pseudo-thermal ghost imaging (PGI) was examined based on the object dimensions in the macroscopic and microscopic regimes. This research shows that an enhanced scaling of the ghost image CNR and resolution from that of the hybrid speckle pattern was observed with the increase in speckle size for a macroscopic object, compared with the use of single-size speckle patterns. For microscopic objects, the hybrid speckle pattern also offered the advantage of retrieving ghost images even if the CNR followed the same trend as the resolution. These results were verified using two different slits with the same transmitted area. In addition, the numerical analysis revealed that the interference of the hybrid speckle pattern was the major factor for a better CNR. Based on these findings, the novel hybrid speckle pattern found in this research provides a possible way for future experiments in PGI to regulate hybrid speckle patterns to obtain a better ghost image quality.

Keywords: ghost imaging; hybrid speckle pattern; image quality

1. Introduction

Pseudo-thermal light generated by scattering laser radiation from a rotating ground glass diffuser has been widely employed in ghost imaging experiments [1–4]. Pseudo-thermal ghost imaging (PGI) is a nonlocal imaging technique that relies on spatial intensity fluctuation correlations to image objects, which allows us to overcome resolution limitations of a few micrometers [5–8]. Here, the spatial intensity fluctuation distribution is produced by the mutual interference of two beams with a random wavefront known as a speckle pattern. The ghost imaging of an unknown object relies on correlating the speckle patterns and corresponding single-pixel signals. Compared to ghost imaging based on entangled photon pairs, PGI is very flexible regarding wavelength, e.g., X-ray ghost imaging has been demonstrated [9–12]. Thus, in recent years, PGI has been investigated extensively [13–17] to overcome the limitations of image quality.

At first, Bennink et al. [4] presented an experimental demonstration of ghost imaging by using a pseudo-thermal light source. Recent studies [18–22] have shown that implementing a speckle-based imaging method is one of the strategies to improve the image quality in PGI. The ghost image quality, e.g., contrast-to-noise ratio (CNR) and resolution, highly depends on the characteristics of the speckle patterns. To be specific, increasing the speckle size results in high CNR reconstructions. In contrast, decreasing the speckle size results in a higher resolution, but with reduced visibility. In our previous results [23], we found that the scaling laws for the CNR of the retrieved ghost images strongly depend on the ratio between the object size and the speckle size of the pseudo-thermal light for the same number of independent iterations. However, because the detector noise is fixed in the PGI experiment system, the detectable signal becomes weaker relative to the noise as the



Citation: Tian, T.; Sun, Z.; Oh, S.; Spielmann, C. Image-Enhanced Pseudo-Thermal Ghost Imaging with Hybrid Speckle Pattern. *Photonics* **2023**, *10*, 709. <https://doi.org/10.3390/photonics10070709>

Received: 11 May 2023

Revised: 14 June 2023

Accepted: 20 June 2023

Published: 21 June 2023



Copyright: © 2023 by the authors. Licensee MDPI, Basel, Switzerland. This article is an open access article distributed under the terms and conditions of the Creative Commons Attribution (CC BY) license (<https://creativecommons.org/licenses/by/4.0/>).

object size decreases to microscale dimensions. Therefore, it becomes very interesting to test the effect of hybrid speckle patterns on enhancing the image quality.

From the principle of PGI, it is known that increasing the intensity fluctuation of the light field on the camera and bucket detector can improve the imaging quality, easing the detector requirements of spatial or time resolution. Fortunately, Zhong et al. [24] and Zerom et al. [21] demonstrated that the high temporal resolution requirements for detectors are reduced by continuously detecting multiple independent speckle patterns without image quality degradation. The image quality can even be improved by using a slow detector for thermal ghost imaging with highly fluctuating thermal speckle patterns. However, these studies mainly focus on thermal ghost imaging with random speckle patterns generated by digital micromirror devices (DMD) and do not focus on ghost imaging with different speckle pattern combinations. Chen et al. [25] presented the possibility of generating multi-correlation-scale speckle patterns to reconstruct the ghost image. Zhou et al. [26] proposed a method to improve the quality of ghost images using a hybrid speckle pattern. In this method, the higher and lower resolution areas of the object could be detected by automatically identifying complex objects composed of different resolution scales. However, it is not the optimal method because the pre-defined speckle patterns may not be the best for the given object. Wang et al. [27] proposed a compressive computational ghost imaging method by using hybrid speckle patterns to retrieve the object. This hybrid speckle pattern is composed of different sizes of speckles that depend on the resolution of the object. However, the DMD-based hybrid speckle pattern used in computational ghost imaging is a temporal or spatial combination, rather than a spatial superposition of hybrid speckles, because DMD is a binary device that can only generate two grayscale values, namely white and black. In addition, they did not discuss the influence of different superimposed combinations of hybrid speckle patterns on the contrast and resolution of ghost imaging. Here, we propose a novel classical ghost imaging method with a hybrid speckle pattern to obtain better image quality and object adaptability.

In this study, we continuously controlled the hybrid speckle patterns using two adjustable apertures in our setup for generating the pseudo-thermal light. With this step, we were able to improve the CNR compared to the single-size speckle pattern approaches. Using objects with different sizes, we verified that these observations were very general. Thus, high-quality ghost imaging can be realized only if the hybrid speckle pattern is carefully adjusted for a given object. The observed scaling can be easily transferred to other spectral ranges and thus will be an important step towards microscopic ghost imaging in the XUV/X-ray regime.

2. Principle and Measurement Setup

2.1. Theory

PGI relies on correlating a measured 2-dimensional intensity speckle pattern to a transmission or reflection scalar value of an object, illuminated by the same speckle pattern. By varying the speckle pattern over time and the simultaneous measurement of the transmitted light through the object, the statistical reconstruction of the image is enabled. Thus, the measured 2D speckle pattern is weighted by the corresponding scalar value of an object in every iteration and is added to the ghost image. The ghost imaging reconstruction algorithm and the measurement of the quality of a ghost image used in this work were published by [14,15],

$$G(x, y) = \frac{1}{N} \sum_{n=1}^N (B - \langle B \rangle) (I(x, y) - \langle I(x, y) \rangle) \quad (1)$$

where the ghost image $G(x, y)$ depends on the measured intensity distribution $I(x, y)$ in the reference beam and N is the total number of iterations. The brackets represent the mean over all the iterations. The total light intensity containing the unknown object's information measured by a single-pixel detector is recorded as B , and B is the integrated

signal over the whole image plane. For each iteration, information about the total integrated intensity of the light transmitted through the object and the spatial intensity distribution in the reference beam is obtained. The ghost image gradually appears while the number of speckle realizations increases.

The randomness of the rotating ground glass diffuser in PGI imposes field fluctuations. A pseudo-thermal ghost image always lies on a noisy background. Thus, the noise in the background of the retrieved image is one of the main obstacles affecting the image quality. Here, we use the CNR to measure the quality of a ghost image, which is calculated from the object signal strength and the background signal strength and normalized to the image noise:

$$CNR = \frac{\langle I_o \rangle - \langle S_i \rangle}{\sigma} \quad (2)$$

where $\langle I_o \rangle$ is the mean signal of the object area, $\langle S_i \rangle$ is the mean signal of the background in the ghost image, and σ is the standard derivation of the image considering noise.

To estimate the spatial resolution of the retrieved ghost image, the slanted-edge method is used. The retrieved ghost image is chosen such that its area is nearly equally covered by the signal and background. The resolution is calculated by fitting an error function according to Ref. [23]. A higher value indicates a lower resolution.

2.2. Experimental Setup

The experimental setup to study the evolution of CNR with speckle patterns is shown in Figure 1. A He-Ne laser and a rotating diffuser constituted a pseudo-thermal light source. Speckle patterns are generated when a laser beam passes through a rotating ground glass. The ground glass is composed of a large number of irregular and independent micro-diffusers. When the laser beam illuminates the ground glass, the widespread presence of numerous small scatterers causes the scattered light field to follow a Gaussian distribution in both the space and time domains. This phenomenon allows for the simulation of the statistical properties of thermal light [28,29]. In order to modify the randomness and achieve a non-Gaussian distribution of light fields, fabrication methods such as laser-write metasurfaces need to be employed [30]. Two unmounted N-BK7 ground glass diffusers (DG10-220—Ø1" Unmounted N-BK7 Ground Glass Diffuser, 220 Grit Thorlabs Inc., Newton, NJ, USA) were selected to generate speckle patterns in our experiment. The rotating diffuser is in the focal plane of the lens of focal length $f = 150$ mm. From $\delta x_0 = \pi \lambda f / \omega_0$ [27,31], different average speckle sizes δx_0 can be obtained by changing the beam waist ω_0 , by controlling the open diameter of aperture 1 and/or aperture 2 from 1.0 mm to 2.25 mm. The different hybrid speckle patterns are generated by adjusting the two aperture diameters. If we close one of the apertures, we can obtain single-size speckle patterns. The typical single-size speckle patterns and hybrid speckle patterns are shown at the bottom of Figure 1. The speckles are separated by a beam splitter, then transmitted by two apertures through the same distance of free-space paths. The angle between the two beams is less than 3° . After the rotating ground glass diffuser, the two beams with different speckle patterns are focused by a lens to hit the camera and the object at the same distance by controlling time-delay mirrors. The reference beam does not interact with the object, and its speckle pattern is recorded using a monochrome industrial CCD camera, with 1200×1600 pixels and an effective pixel size of $5.86 \mu\text{m} \times 5.86 \mu\text{m}$, which is much smaller than the speckle size of δx_0 . In the test beam, the laser passes through the object and is recorded by a bucket detector (single-pixel detector). Here, the error in the propagation lengths between the reference beam and test beam paths is in the order of a few millimeters. Two laser-cut μ -shaped transmitting objects were used as the test objects for ghost imaging. Their actual shape and sizes are also shown in Figure 1. The widths of the vertical bar of the letter “ μ ” in objects 1 and 2 are $120 \mu\text{m}$ and $60 \mu\text{m}$, respectively. Correspondingly, the areas of objects 1 and 2 are calculated as $\sim 180 \times 10^3 \mu\text{m}^2$ and $\sim 77 \times 10^3 \mu\text{m}^2$, respectively. It is worth noting that the main objective of this study is to explore the ghost imaging principles

of hybrid speckle patterns. The size of the speckles and objects involved can be adjusted according to practical requirements.

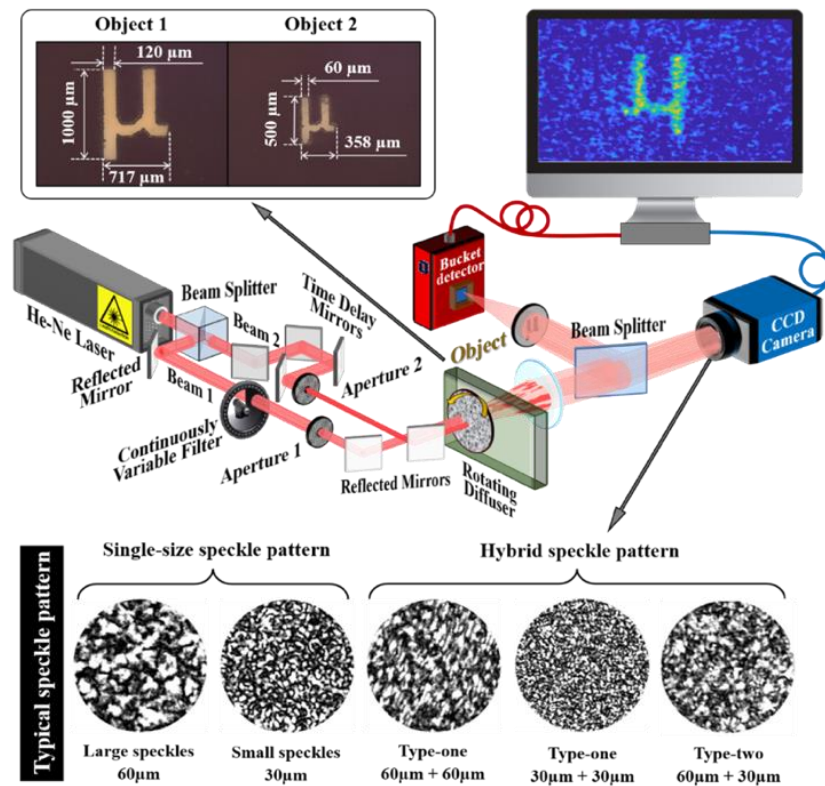


Figure 1. Schematics of PGI setup with hybrid speckle pattern. The time-delay module is used to ensure that the two beams produce speckle patterns at the same optical path length. The rotating diffuser is used to impress two spatially random speckle patterns onto the laser field.

3. Experiment and Simulation Results

3.1. Experimental Results and Discussion

Starting with object 1, the speckle size was increased from 36 μm to 60 μm in five steps, followed by reconstruction with 10,000 iterations under the same conditions. In the traditional single-size speckle pattern imaging condition, the retrieved ghost image CNR-dependent speckle size was found to be in good agreement with [18–23], which indicates a growth of the CNR and a reduced resolution proportional to the speckle size in Figure 2 (black line with solid squares and black line with hollow squares). The highest CNR ghost image was obtained with the largest speckle size of 60 μm . The best resolution was obtained with the smallest speckle size of 36 μm .

To verify the image quality evolution with the hybrid speckle pattern, we designed two types of combinations experiments as presented in Table 1. For the type-one hybrid speckle pattern, aperture 1 and aperture 2 had the same diameter. In this case, the hybrid speckle patterns were built up by two similar speckle patterns. The speckle size was increased from 36 μm to 60 μm in five steps, so we had five kinds of hybrid speckle patterns for ghost imaging. For the type-two hybrid speckle pattern, aperture 1 and aperture 2 had different diameters. Because the highest CNR can be obtained by using a $\sim 60 \mu\text{m}$ speckle size in a single-size speckle pattern imaging condition, we fixed the diameter of aperture 2 at 1 mm diameter to obtain a $\sim 60 \mu\text{m}$ speckle size. The speckles after aperture 1 were stepwise increased from 36 μm to 60 μm .

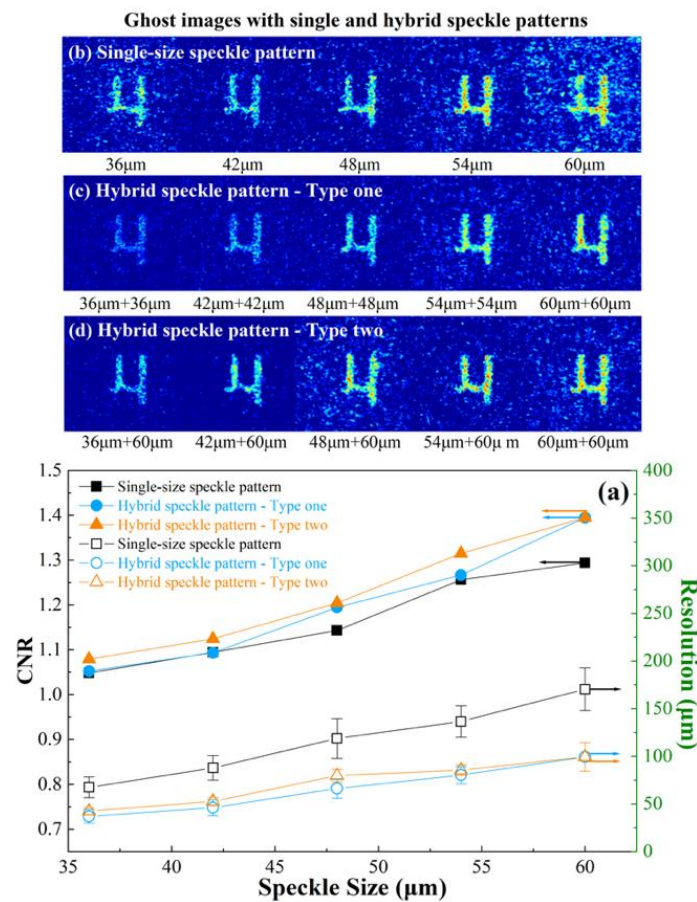


Figure 2. Retrieved CNR and resolution vs. speckle patterns for object 1. (a) Retrieved CNR of the μ -shaped object increases with higher speckle size, and resolution worsens with higher speckle size; (b) ghost images with single-size speckle pattern; (c) ghost images with type-one hybrid speckle pattern; (d) ghost images with type-two hybrid speckle pattern. Note: ghost images of an object are imaged in the same dynamic range.

Table 1. Hybrid speckle pattern combinations for object 1.

Sequence	Pattern I		Pattern II		Pattern III		Pattern IV		Pattern V	
Aperture	1	2	1	2	1	2	1	2	1	2
Type-one (μm)	36	36	42	42	48	48	54	54	60	60
Type-two (μm)	36	60	42	60	48	60	54	60	60	60

To clearly understand and generalize the influence of hybrid speckle patterns on the CNR of the retrieved ghost images for an object of a given size, we evaluated the CNR and resolution as a function of the two types of hybrid speckle patterns. For easy comparison between the CNR and resolution resulting from a single-size speckle pattern, we plot the speckle size after aperture 1 with a common abscissa in Figure 2a. The corresponding marked retrieved ghost images are exhibited in Figure 2b–d. In Figure 2 (blue line with solid circles), we summarize the dependence of the CNR on the type-one hybrid speckle pattern. The corresponding resolution is shown in Figure 2 (blue line with hollow circles). The scaling of the CNR and resolution undergoes the same evolution with the single-size speckle pattern imaging. In most cases, this hybrid speckle superimposed by the same speckle shows a clear advantage in imaging quality. This advantage is further improved

when changing to a type-two hybrid speckle pattern. As we can see from Figure 2 (orange line with solid triangles), the CNR of the retrieved ghost images is slightly higher than the type-one hybrid speckle pattern for ghost imaging because of the larger speckles. At the same time, the resolution is slightly lower than that of the type-one hybrid speckle pattern in Figure 2 (orange line with hollow triangles).

These observations implied that the large speckles in the hybrid speckle pattern contributed substantially to the improvement of the CNR of the ghost images, and the small speckles were also helpful to the improvement of resolution during the ghost imaging reconstruction. First, we used single-size speckles for ghost imaging and selected the speckle size that achieved the highest CNR as one size of speckle in the hybrid speckle field. Here, the speckles with optimal size always provided the most benefits to the improvement of the CNR in ghost imaging with the hybrid speckle pattern. On one hand, when the two optimized speckles were used in the hybrid speckle pattern, the CNR reached its maximum value. On the other hand, because of the coherence of the light field, the hybrid speckle field produced finer interference fringes in some parts of the hybrid speckle field where the speckles overlapped. These finer stripes provided a significant contribution to the increase in resolution. Thus, the ghost imaging resolution of the hybrid speckle pattern was higher than that of the single-size speckle pattern.

This indicated that an optimal hybrid speckle pattern existed in the PGI, for which the maximum CNR with a better resolution can be achieved for the given object size. In the experiment, we separately compared the two beams with the same speckle size for ghost imaging, and the image quality was almost the same. Subsequently, in the hybrid speckle pattern ghost imaging experiment, we believed that fixing the speckle size of any one of the beams would not affect the experimental results. Moreover, this scaling was easily observed from the ghost images represented by false color, as in Figure 2b–d. It is worth noting that the retrieved ghost images that are visible to the naked eye are not exactly the same as the image with the highest CNR, because the CNR takes full image noise into account (given by Equation (2)). Therefore, we used both CNR and resolution to estimate the image quality.

By reducing the size of the object to the microscopic scale, the speckle size became comparable to the dimension of the object. The CNR scaling of object 2, with features in the speckle size range, exhibited a different scaling compared to object 1. Here, we used a set of smaller-sized speckle patterns to study the properties of the retrieved ghost images with hybrid speckle patterns. It was observed that the CNR showed an increasing trend from the speckle size of 30 μm . Then, it reached a maximum of 36 μm , following which it dropped continuously, as shown in Figure 3 (black line with solid squares). The reason for the reversed trend is that the noise level of the photodiode is the major limitation to the growth of the CNR for large speckle sizes. The lower transmission reduces the margin between typical signal levels, and the noisy background of the photodiode results in a shift from the maximum CNR with respect to smaller speckle sizes. With the increase in noise level, this effect becomes increasingly prominent in fields with smaller speckle sizes [27].

In addition to the CNR, the resolution of the retrieved images was evaluated. Different from the CNR, the resolution is mainly affected by the speckle size, i.e., the resolution increases with smaller speckle sizes independent of the dimension of the object. However, due to the limitation of the pixel size of the camera, the resolution will not increase further. Therefore, in the case of object 2, because of the limited detection capabilities of the system, decreasing the speckle size resulted in a higher CNR and a higher resolution. Moreover, the resolution itself was limited by the pixel size of the imaging device and was comparable to the resolution achieved with shadow grams of object 2. Thus, the declining trend of the resolution of object 2 was slower than that of object 1.

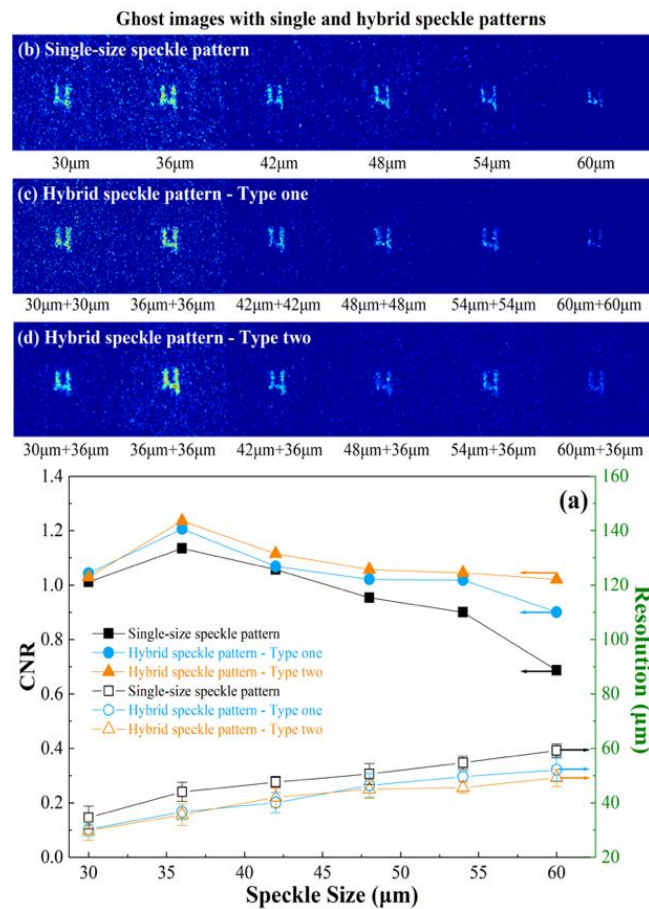


Figure 3. Retrieved CNR and resolution vs. speckle patterns for object 2. (a) Retrieved CNR of the μ -shaped object decreases with higher speckle size after $\sim 36\mu\text{m}$, and resolution worsens with higher speckle size; (b) ghost images with single-size speckle pattern; (c) ghost images with type-one hybrid speckle pattern; (d) ghost images with type-two hybrid speckle pattern. Note: ghost images of an object are imaged in the same dynamic range.

As presented in Table 2, we also provide two types of combination experiments to verify the image quality evolution of hybrid speckle patterns. Because of the increase in resolution with smaller speckle sizes, which is independent of the dimension of the object, the trade-off must only be considered for object 1. On the contrary, in the case of object 2, because of the limited detection capabilities of the system, decreasing the speckle size resulted in a higher CNR and a higher resolution. In this way, for type-two hybrid speckle pattern, aperture 2 fixed at a 2 mm diameter to obtain a $\sim 36\mu\text{m}$ speckle size obtained the highest CNR with a higher resolution in single-size speckle pattern imaging condition. The speckles after aperture 1 increased from $30\mu\text{m}$ to $60\mu\text{m}$ in six steps. The type-one hybrid speckle pattern remained unchanged. In Figure 3 (blue line with solid circles and orange line with solid triangles), we summarize the dependence of the CNR on type-one and -two hybrid speckle patterns, and the corresponding resolutions are shown in Figure 3 (blue line with hollow circles and orange line with hollow triangles). Both CNRs with hybrid speckle patterns decrease rapidly with increasing speckle size after the pattern 2 series because of the negligible bucket detector noise signal. For the type-two hybrid speckle pattern, because it has smaller speckles, it is easier to achieve ghost imaging with a high CNR and resolution in this case.

Table 2. Hybrid speckle pattern combinations for object 2.

Sequence	Pattern I		Pattern II		Pattern III		Pattern IV		Pattern V		Pattern VI	
Apertures	1	2	1	2	1	2	1	2	1	2	1	2
Type-1 (μm)	30	30	36	36	42	42	48	48	54	54	60	60
Type-2 (μm)	30	36	36	36	42	36	48	36	54	36	60	36

Comparing the results with the single-size speckle pattern, the following conclusion can be derived: the scaling of the retrieved ghost image CNR and resolution strongly depend on the combination of the hybrid speckle patterns for the same number of independent iterations. The method of using the hybrid speckle pattern instead of the single-size speckle pattern to improve the quality of ghost imaging can be extended from macroscopic to microscopic imaging.

To generalize our observations in PGI, the experiment was repeated with two slits with the same transmission area. For comparison, two slits with the size of 1200 μm × 150 μm and 517 μm × 150 μm, respectively, were used. Figures 4 and 5 show the experimental results of the CNRs for test slits 1 and 2, corresponding to objects 1 and 2. The ghost images for the two slits were retrieved by 10,000 independent iterations of the corresponding speckle patterns. The agreement between the estimated CNR and resolution for the two completely differently shaped objects with the same transparent area was excellent. A slight discrepancy was observed because of the deviation of the object area selected for the measurement, and some uncertainties in the estimated area of the “μ” and/or small errors in setting the slit width.

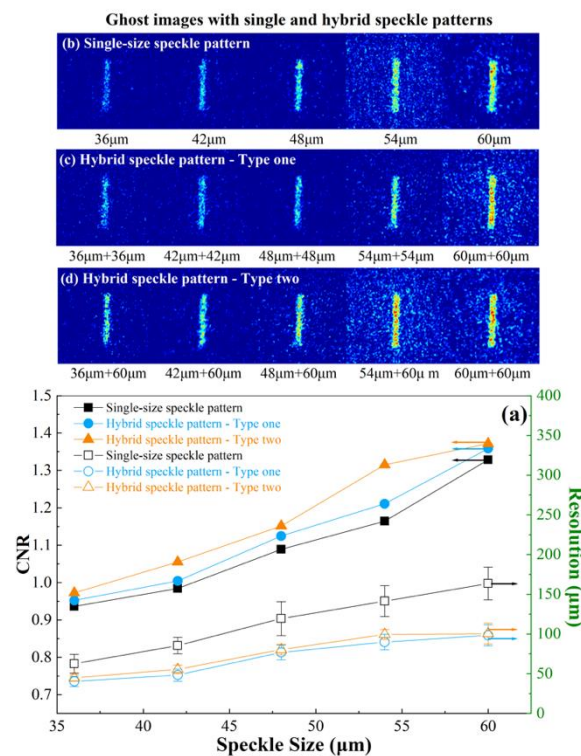


Figure 4. Retrieved CNR and resolution vs. speckle patterns for test slit 1. (a) Retrieved CNR of the μ-shaped object increases with higher speckle size, and resolution worsens with higher speckle size; (b) ghost images with single-size speckle pattern; (c) ghost images with type-one hybrid speckle pattern; (d) ghost images with type-two hybrid speckle pattern. Note: ghost images of an object are imaged in the same dynamic range.

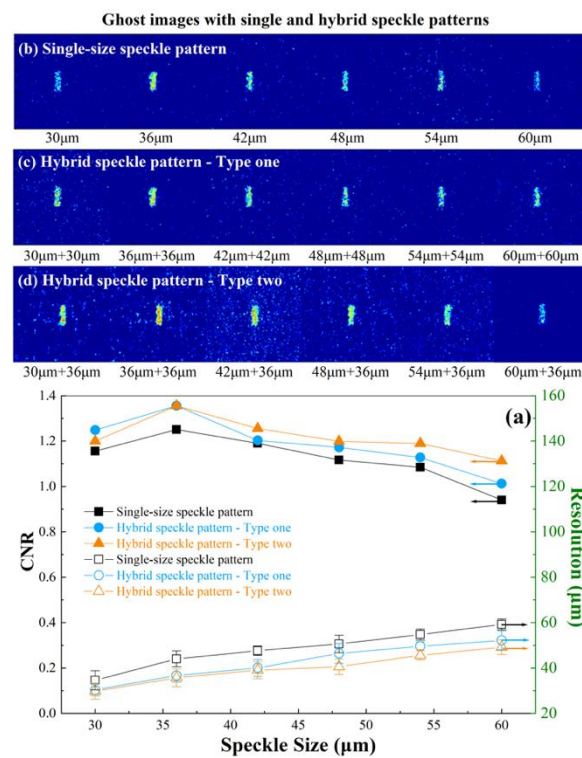


Figure 5. Retrieved CNR and resolution vs. speckle patterns for test slit 2. (a) Retrieved CNR of the μ -shaped object decreases with higher speckle size after $\sim 36 \mu\text{m}$, and resolution worsens with higher speckle size; (b) ghost images with single-size speckle pattern; (c) ghost images with type-one hybrid speckle pattern; (d) ghost images with type-two hybrid speckle pattern. Note: ghost images of an object are imaged in the same dynamic range.

3.2. Simulation Results

To validate the experimentally observed enhanced image quality of hybrid speckle patterns, the interference speckle pattern model was developed to simulate the observed behavior. It can independently vary the interference parameters over a wide range to identify their role in the observed scaling of the CNR for hybrid speckle patterns. First, we implemented an expression to numerically generate random speckle fields based on the interference of two monochromatic waves [31]. Then, we developed the hybrid speckle pattern model to reconstruct the ghost image. Figure 6 shows the reconstruction images of the slit with the size of $1200 \mu\text{m} \times 150 \mu\text{m}$ for 25 different combinations of hybrid speckle patterns, ranging from a speckle size of $12 \mu\text{m}$ to $60 \mu\text{m}$. The retrieved ghost images are given by the combination of the speckles, both in abscissa and ordinate. We also present 19 retrieved ghost images with single-size speckle patterns obtained by only one optical path for comparison. The speckle size of $0 \mu\text{m}$ means the optical path has no contribution to the ghost imaging reconstruction. In this case, we obtained the ghost image with a single-size speckle pattern. Since the two optical paths use the same speckle for ghost imaging, the imaging quality is almost the same as in the experiment. Thus, we considered that the contribution of the two optical paths to ghost imaging must be the same in the simulation. By comparing the simulation results with the experimental results described above, two types of hybrid speckle patterns were identified for a given combination of hybrid speckle patterns. The retrieved ghost image of the type-two hybrid speckle pattern exhibited better features than the type-one hybrid speckle pattern, resulting in a slightly higher CNR. Moreover, the retrieved ghost images of the hybrid speckle pattern had a higher CNR than those of the single-size speckle pattern.

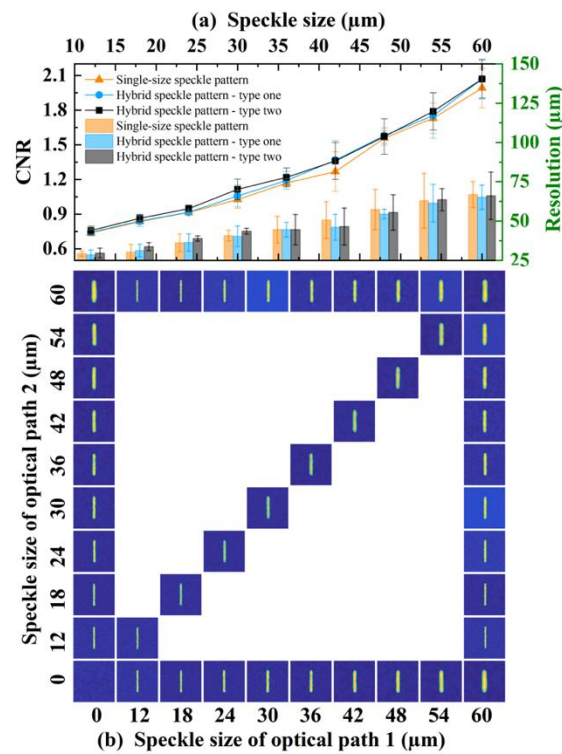


Figure 6. Results of the hybrid-speckle-pattern-dependent CNR simulation with 20 μm spacing of interference fringes. (a) Calculated CNR and resolution of the ghost images as a function of type-one, -two hybrid speckle pattern, and single-size speckle pattern; (b) retrieved ghost images as a function of hybrid speckle pattern and single-size speckle pattern. For type-one hybrid speckle patterns, we use the speckle patterns hybridized with a 60 μm speckle size for simulation. For the type-two hybrid speckle pattern, we use the speckle patterns hybridized with speckles of the same size for simulation. All data are averaged after 10 calculations with 5000 iterations.

It has been proven by Ref. [23] that the anomalous evolution law of the speckles and image quality for a smaller object is only caused by the detector noise level. Thus, we only use object 2 for simulation. It is worth noting that we set the spacing of interference fringes of the simulated hybrid speckle pattern close to the experiment. We did not discuss the influence of the spacing of interference fringes for hybrid speckle patterns on image quality in the experiment, but we made the comparison in the simulation.

To further analyze the influence of the hybrid speckle pattern on ghost image quality, we simulated the hybrid speckle pattern with the different spacing of interference fringes in Figure 7a and corresponding retrieved ghost images in Figure 7b. The theory of the spacing of interference fringes in the simulation can be explained by Young’s double-slit interference experiment [31]. Because the best image quality was obtained by pattern V of the type-one hybrid speckle pattern (60 μm + 60 μm) when the spacing of interference fringes was 20 μm in Figure 6, we chose it for the simulation. We first made a comparison with the single-size speckle pattern with a speckle size of 60 μm . It is clear to see that the quality of the retrieved ghost images with hybrid speckle patterns having 20 μm spacing of interference fringes is better than the single-speckle pattern in Figure 7a,c. This behavior can be attributed to the interference between the hybrid speckles, which were strongly modified in the speckle fields. We also simulated pattern V of the type-one hybrid speckle pattern without interference fringes. The calculated CNR and resolution of the retrieved ghost images of the hybrid speckle pattern without interference fringes were close to the single-speckle pattern in Figure 7d. Thus, the hybrid speckle pattern without interference fringes was almost equivalent to a random speckle pattern with a fixed single size.

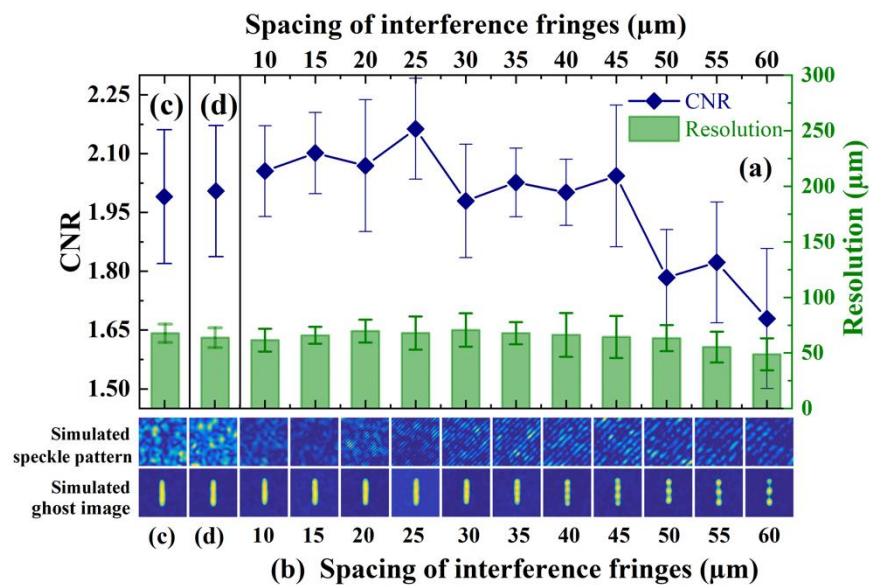


Figure 7. Results of pattern V of the type-one hybrid speckle pattern are dependent on the CNR corresponding to the simulation of different spacings of interference fringes. (a) Calculated CNR and resolution of the retrieved ghost images as a function of the spacing of interference fringes of the hybrid speckle pattern; (b) retrieved ghost image of pattern V corresponds to the simulated speckle pattern with different spacings of interference fringes; (c) calculated CNR and resolution of the retrieved ghost image of the single-size speckle pattern of 60μm, corresponding simulated speckle pattern, and the retrieved ghost image; (d) calculated CNR and resolution of the retrieved ghost image of the hybrid speckle pattern of 60 μm + 60 μm without interference fringes, corresponding simulated speckle pattern, and the retrieved ghost image. All data are averaged after 10 calculations with 5000 iterations.

Then, we studied the evolution of the calculated CNR and resolution of the retrieved ghost images with the spacing of interference fringes of the hybrid speckle pattern. It was observed that the CNR showed a slight increase for a small spacing of interference fringes until it reached a maximum, following a stepwise decrease, as shown in Figure 7a. Different from the CNR, the resolution did not significantly vary. Thus, the shape of the retrieved ghost images worsened above a 40 μm interference fringe spacing. In Figure 7b, we show the corresponding speckle patterns for different interference fringe distances. The ghost imaging images obtained using these speckle patterns are also given in Figure 7b. To make the simulation closer to the experiment, we selected the spacing of interference fringes with 20 μm to simulate the ghost imaging effect of the hybrid speckle pattern. However, it can be seen from the results in Figure 7b that it was not the best choice for acquiring a better image quality. In the future, we can further optimize our experiments when the spacing of interference fringes of the hybrid speckle pattern is close to 25 μm by adjusting the parameters of the input laser.

The hybrid speckle patterns show advantages in improving the image quality of PGI, but also has a limitation for practical applications due to the necessity of the precise control of the arm lengths in the experimental setup. With the help of the correlation function introduced in Refs. [32–34], we can classify the different speckle pattern states by their robustness to deviations from the ideal setup. We simulated the correlation evolution dependent on the error in propagation lengths between the reference and test beam with the hybrid speckle pattern and single-size speckle pattern. As seen in Figure 8, as the single-speckle size increased, the correlation factor increased. The correlation of the single-size speckle pattern was significantly higher than the hybrid speckle pattern within a large error in the range of propagation lengths. For the type-one hybrid speckle pattern (60 μm + 60 μm), the correlation factor did not drop significantly over a wide range, although it was also slightly lower than the correlation factor for single-speckle sizes larger

than 48 μm . On the contrary, for the other hybrid speckle patterns, the correlation factor was lower than the single-speckle size of 18 μm , even close to the correlation factor of the minimum single-speckle size of 12 μm . Especially for the type-two hybrid speckle pattern (12 μm + 60 μm), the correlation appeared to be greatly reduced after the error exceeded a few million meters. This means that for the vast majority of hybrid speckle patterns used in PGI, the length error between the reference and test beams must be precisely controlled.

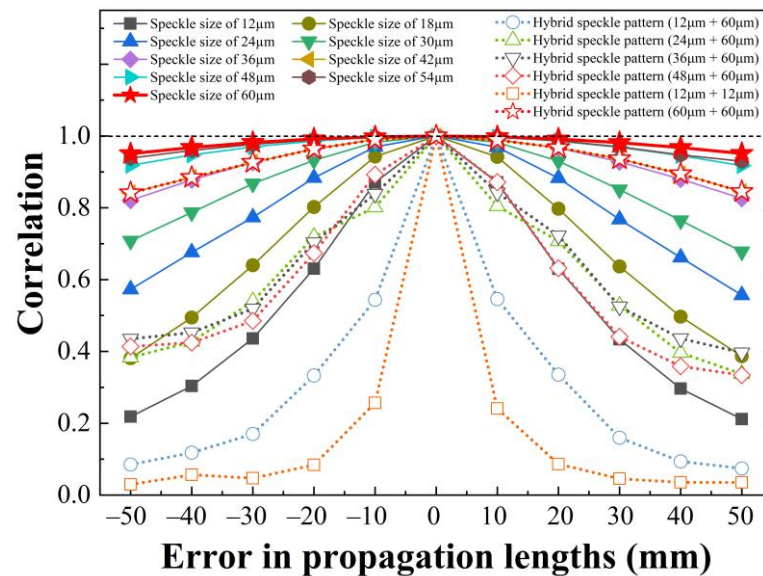


Figure 8. Simulation of the correlation factor dependent on the error in propagation lengths with different speckle patterns.

4. Conclusions

We analyzed the role of the hybrid speckle pattern on the achievable CNR and resolution in PGI. From our experiments, we obtained the scaling laws for the CNR and resolution of the retrieved ghost images in both type-one and -two hybrid speckle patterns for the same number of independent iterations. For comparison, the CNR and resolution scaling were observed for two objects of different shapes with the same transmittance. The results showed that the ghost imaging results using rectangular slits and more complex structures were consistent, that is, the CNR was shape-independent. For all the samples, because of the impact of the speckle size on the CNR and resolution, as well as the fine interference fringes produced by the coherence effect of the partial speckles in the hybrid speckle pattern, the ghost imaging quality obtained by using the hybrid speckle pattern was always better.

An analysis of our simulation unambiguously identified the hybrid speckle pattern with interference as the major parameter for the increase in CNR. The influence of the interference of the hybrid speckle pattern on CNR behavior has been theoretically discussed in the field of PGI. The hybrid speckle pattern has better adaptability to an object compared to the single-size speckle pattern, because the hybrid speckle pattern can be easily generated by the interference of two random speckle fields and is convenient to use in practical applications. In addition, the novel hybrid speckle pattern found in this research will be of great importance in future experiments on microscopic ghost imaging in regulating speckle sizes and their combinations to obtain better image quality.

Author Contributions: T.T. and Z.S. contributed equally to this research, and they analyzed the experimental phenomena and results together. T.T. designed and performed the numerical investigation. Z.S. conceived the idea and conducted the experiments. S.O. participated in discussions and contributed to preliminary experiments. C.S. reviewed the manuscript and supervised the project. All authors have read and agreed to the published version of the manuscript.

Funding: This research was funded by Deutsche Forschungsgemeinschaft (DFG, German Research Foundation) under Germany's Excellence Strategy—EXC 2051 (Project-ID 390713860), “Balance of the Microverse”, and the Fundamental Research Funds for the Central Universities (D5000220481).

Institutional Review Board Statement: Not applicable.

Informed Consent Statement: Not applicable.

Data Availability Statement: Data underlying the results presented in this paper are not publicly available at this time but may be obtained from the authors upon reasonable request.

Conflicts of Interest: The authors declare no conflict of interest. The funders had no role in the design of the study; in the collection, analyses, or interpretation of data; in the writing of the manuscript; or in the decision to publish the results.

References

1. Asakura, T. Spatial Coherence of Laser Light Passed through Rotating Ground Glass. *Opto Electron.* **1970**, *2*, 115–123. [[CrossRef](#)]
2. Estes, L.E.; Narducci, L.M.; Tuft, R.A. Scattering of Light from a Rotating Ground Glass. *JOSA* **1971**, *61*, 1301–1306. [[CrossRef](#)]
3. Kumar, A.; Banerji, J.; Singh, R.P. Intensity Correlation Properties of High-Order Optical Vortices Passing through a Rotating Ground-Glass Plate. *Opt. Lett.* **2010**, *35*, 3841–3843. [[CrossRef](#)] [[PubMed](#)]
4. Bennink, R.S.; Bentley, S.J.; Boyd, R.W. “Two-Photon” Coincidence Imaging with a Classical Source. *Phys. Rev. Lett.* **2002**, *89*, 113601. [[CrossRef](#)] [[PubMed](#)]
5. Ferri, F.; Magatti, D.; Gatti, A.; Bache, M.; Brambilla, E.; Lugiato, L.A. High-Resolution Ghost Image and Ghost Diffraction Experiments with Thermal Light. *Phys. Rev. Lett.* **2005**, *94*, 183602. [[CrossRef](#)]
6. D’Angelo, M.; Valencia, A.; Rubin, M.H.; Shih, Y. Resolution of Quantum and Classical Ghost Imaging. *Phys. Rev. A* **2005**, *72*, 013810. [[CrossRef](#)]
7. Cao, D.-Z.; Xiong, J.; Zhang, S.-H.; Lin, L.-F.; Gao, L.; Wang, K. Enhancing Visibility and Resolution in N Th-Order Intensity Correlation of Thermal Light. *Appl. Phys. Lett.* **2008**, *92*, 201102. [[CrossRef](#)]
8. Gong, W.; Han, S. High-Resolution Far-Field Ghost Imaging via Sparsity Constraint. *Sci. Rep.* **2015**, *5*, srep09280. [[CrossRef](#)]
9. Yu, H.; Lu, R.; Han, S.; Xie, H.; Du, G.; Xiao, T.; Zhu, D. Fourier-Transform Ghost Imaging with Hard X rays. *Phys. Rev. Lett.* **2016**, *117*, 113901. [[CrossRef](#)]
10. Pelliccia, D.; Rack, A.; Scheel, M.; Cantelli, V.; Paganin, D.M. Experimental X-ray Ghost Imaging. *Phys. Rev. Lett.* **2016**, *117*, 113902. [[CrossRef](#)]
11. Schori, A.; Shwartz, S. X-ray Ghost Imaging with a Laboratory Source. *Opt. Express* **2017**, *25*, 14822–14828. [[CrossRef](#)]
12. Zhang, A.-X.; He, Y.-H.; Wu, L.-A.; Chen, L.-M.; Wang, B.-B. Tabletop X-Ray Ghost Imaging with Ultra-Low Radiation. *Optica* **2018**, *5*, 374–377. [[CrossRef](#)]
13. Gatti, A.; Bache, M.; Magatti, D.; Brambilla, E.; Ferri, F.; Lugiato, L.A. Coherent Imaging with Pseudo-Thermal Incoherent Light. *J. Mod. Opt.* **2006**, *53*, 739–760. [[CrossRef](#)]
14. Zhang, P.; Gong, W.; Shen, X.; Huang, D.; Han, S. Improving Resolution by the Second-Order Correlation of Light Fields. *Opt. Lett.* **2009**, *34*, 1222–1224. [[CrossRef](#)]
15. Han, S.; Yu, H.; Shen, X.; Liu, H.; Gong, W.; Liu, Z. A Review of Ghost Imaging via Sparsity Constraints. *Appl. Sci.* **2018**, *8*, 1379. [[CrossRef](#)]
16. Ma, S.; Liu, Z.; Wang, C.; Hu, C.; Li, E.; Gong, W.; Tong, Z.; Wu, J.; Shen, X.; Han, S. Ghost Imaging LiDAR via Sparsity Constraints Using Push-Broom Scanning. *Opt. Express* **2019**, *27*, 13219–13228. [[CrossRef](#)] [[PubMed](#)]
17. Sun, Z.; Tuitje, F.; Spielmann, C. Improving the Contrast of Pseudo-thermal Ghost Images Based on the Measured Signal Distribution of Speckle Fields. *Appl. Sci.* **2021**, *11*, 2621. [[CrossRef](#)]
18. Ferri, F.; Magatti, D.; Sala, V.G.; Gatti, A. Longitudinal Coherence in Thermal Ghost Imaging. *Appl. Phys. Lett.* **2008**, *92*, 261109. [[CrossRef](#)]
19. Gatti, A.; Magatti, D.; Ferri, F. Three-Dimensional Coherence of Light Speckles: Theory. *Phys. Rev. A* **2008**, *78*, 063806. [[CrossRef](#)]
20. Magatti, D.; Gatti, A.; Ferri, F. Three-Dimensional Coherence of Light Speckles: Experiment. *Phys. Rev. A* **2009**, *79*, 053831. [[CrossRef](#)]
21. Zerom, P.; Shi, Z.; O’Sullivan, M.N.; Chan, K.W.C.; Krogstad, M.; Shapiro, J.H.; Boyd, R.W. Thermal Ghost Imaging with Averaged Speckle Patterns. *Phys. Rev. A* **2012**, *86*, 063817. [[CrossRef](#)]
22. Jue, W.; Renlong, Y.; Yu, X.; Yanming, S.; Yanru, C.; Qi, Z. Ghost Imaging with Different Speckle Sizes of Thermal Light. *J. Opt. Soc. Korea* **2016**, *20*, 8–12. [[CrossRef](#)]
23. Sun, Z.; Tuitje, F.; Spielmann, C. Toward High Contrast and High-Resolution Microscopic Ghost Imaging. *Opt. Express* **2019**, *27*, 33652–33661. [[CrossRef](#)] [[PubMed](#)]
24. Ya-Jun, Z.; Jiao, L.; Wen-Qiang, L.; Sheng-Mei, Z. Multiple Speckle Patterns Differential Compressive Ghost Imaging. *Acta Phys. Sin.* **2015**, *64*, 014202. [[CrossRef](#)]
25. Chen, M.; Li, E.; Han, S. Application of Multi-Correlation-Scale Measurement Matrices in Ghost Imaging via Sparsity Constraints. *Appl. Opt.* **2014**, *53*, 2924–2928. [[CrossRef](#)]

26. Zhou, C.; Huang, H.; Liu, B.; Song, L. Hybrid Speckle-Pattern Compressive Computational Ghost Imaging. *Acta Opt. Sin.* **2016**, *36*, 0911001. [[CrossRef](#)]
27. Wang, X.; Tao, Y.; Yang, F.; Zhang, Y. An Effective Compressive Computational Ghost Imaging with Hybrid Speckle Pattern. *Opt. Commun.* **2020**, *454*, 124470. [[CrossRef](#)]
28. Martienssen, W.; Spiller, E. Coherence and Fluctuations in Light Beams. *Am. J. Phys.* **1964**, *32*, 919–926. [[CrossRef](#)]
29. Zhou, L.; Liu, S.; Zhong, T. A Comprehensive Review of Optical Diffusers: Progress and Prospects. *Nanoscale* **2023**, *15*, 1484–1492. [[CrossRef](#)]
30. Zhu, X.; Engelberg, J.; Remennik, S.; Zhou, B.; Pedersen, J.N.; Uhd Jepsen, P.; Levy, U.; Kristensen, A. Resonant Laser Printing of Optical Metasurfaces. *Nano Lett.* **2022**, *22*, 2786–2792. [[CrossRef](#)]
31. Born, M.; Wolf, E. *Principles of Optics: Electromagnetic Theory of Propagation, Interference and Diffraction of Light*; Elsevier: Amsterdam, The Netherlands, 2013; ISBN 1-4831-0320-X.
32. Glauber, R.J. The Quantum Theory of Optical Coherence. *Phys. Rev.* **1963**, *130*, 2529. [[CrossRef](#)]
33. Ragy, S.; Adesso, G. Nature of Light Correlations in Ghost Imaging. *Sci. Rep.* **2012**, *2*, 651. [[CrossRef](#)] [[PubMed](#)]
34. Moreau, P.-A.; Toninelli, E.; Gregory, T.; Padgett, M.J. Ghost Imaging Using Optical Correlations. *Laser Photonics Rev.* **2018**, *12*, 1700143. [[CrossRef](#)]

Disclaimer/Publisher’s Note: The statements, opinions and data contained in all publications are solely those of the individual author(s) and contributor(s) and not of MDPI and/or the editor(s). MDPI and/or the editor(s) disclaim responsibility for any injury to people or property resulting from any ideas, methods, instructions or products referred to in the content.